Cooperative Motion of Active Brownian Spheres in Three-Dimensional Dense Suspensions

Adam Wysocki, Roland G. Winkler and Gerhard Gompper

Theoretical Soft Matter and Biophysics, Institute for Advanced Simulation and Institute of Complex Systems, Forschungszentrum Jülich, 52425 Jülich, Germany

Abstract –The structural and dynamical properties of suspensions of self-propelled Brownian particles of spherical shape are investigated in three spatial dimensions. Our simulations reveal a phase separation into a dilute and a dense phase, above a certain density and strength of self-propulsion. The packing fraction of the dense phase approaches random close packing at high activity, yet the system remains fluid. Although no alignment mechanism exists in this model, we find long-lived cooperative motion of the particles in the dense regime. This behavior is probably due to an interface-induced sorting process. Spatial displacement correlation functions are nearly scale-free for systems with densities close to or above the glass transition density of passive systems.

Introduction. – Assemblies of intrinsically active objects, sometimes called *living fluids*, represent an exceptional class of non-equilibrium systems. Examples range from the macroscopic scale of human crowds to the microscopic scale of cells and motile microorganisms such as bacteria [1, 2]. A generic phenomenon of dense living fluids is the emergence of self-organized large-scale dynamical patterns like vortices, swarms, networks, or self-sustained turbulence [3, 4]. This intriguing dynamical behavior is a consequence of the complex interplay of self-propulsion, internal or external noise, and many-body interactions.

The understanding of the collective behavior requires the characterization of the underlying physical interaction mechanisms. Experiments and simulations indicate that alignment induced by particle interactions, e.g., inelastic collisions between elongated objects [4–6] or hydrodynamic interactions [7], lead to clustering and collective motion. Studies of rodlike self-propelled particles in two dimensions (2D) revealed mobile clusters and a variety of other dynamical phases [4–6]. In contrast, systems of disclike particles in 2D, which lack an alignment mechanism, do not form any ordered moving states. Yet, they exhibit an activity-induced phase transition. At lower densities small, transient clusters appear [8–11]. Above a critical density, the system separates into a dense and a dilute phase [8, 12–14]. The dense phase exhibits a crystalline order with a slow dynamics, mainly due to movements

of dislocations [10, 12]. Less attention has been paid to three-dimensional (3D) suspensions of spherical (colloid-like) active particles (with the exception of a very recent numerical [15] and theoretical work [16]). In such systems, the question naturally arises, whether a collective behavior emerges despite the particles lack any aligning interactions. In this letter, we present simulation results of the emergent structure and dynamics of motile spherical particles in 3D—as a generic model of non-aligning self-driven particles. We find that an isotropic system phase separates into a dilute, gas-like phase, and a dense, liquid-like phase at sufficiently large activity. Inside the dense phase, the particles exhibit collective motion—in the form of jets and swirls—even at densities very close to random close packing (RCP). Although a global polar order is absent in the system, long-lived cooperative motion with nearly scale-free correlations emerge.

Model. – We model an active particle as a hard-sphere-like particle which is propelled with constant velocity V_0 along its orientation vector $\mathbf{e}$ in 3D [8,12,17]. Its translational motion is described by

$$\dot{\mathbf{r}} = V_0\mathbf{e} + \mathbf{F}/\gamma_t + \boldsymbol{\eta}, \tag{1}$$

where $\dot{\mathbf{r}}$ is the velocity, $\mathbf{F}$ the total interparticle force, and $\boldsymbol{\eta}$ a Gaussian white-noise random velocity, with $\langle\boldsymbol{\eta}\rangle = 0$ and $\langle\boldsymbol{\eta}_i(t)\boldsymbol{\eta}_j(t')\rangle = 2D_t\mathbf{1}\delta_{ij}\delta(t-t')$. The translational dif-
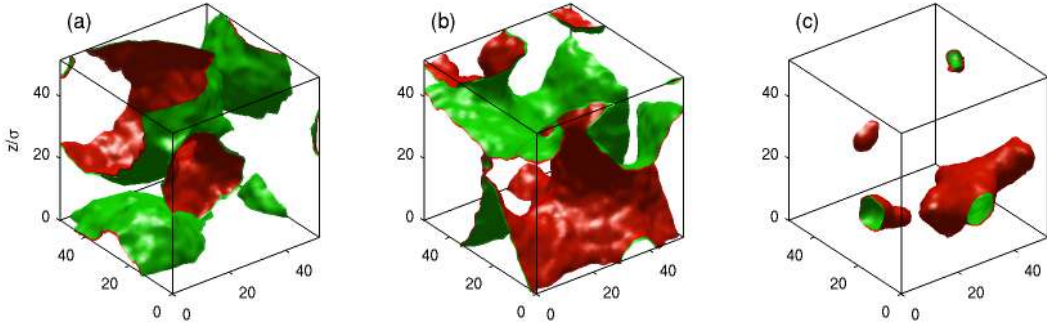
Fig. 1: (color online) Snapshots of the gas-liquid interface of a system (a,b) just above the clustering transition ($\phi = 0.3375$ and $\phi = 0.4$) and (c) at a high density ($\phi = 0.6$). The red isodensity surfaces is drawn at $\phi_{loc} = 0.54$, the green at $\phi_{loc} = 0.5$. See also movies `movie1.avi` and `movie2.avi`.

fusion coefficient D_t is related to the frication coefficient γ_t via $D_t = k_B T/\gamma_t$. The force follows from a steep (shifted) Yukawa-like potential $V(r)/k_B T = 5e^{-\kappa(r-\sigma)}/[\kappa(r-\sigma)]$ for $r > \sigma$, $V(r) = \infty$ for $r \leq \sigma$, and $V(r) = 0$ for $r > 1.083\sigma$, with particle diameter σ and $\kappa\sigma = 60$. The orientation **e** performs a random walk according to $\dot{\mathbf{e}} = \boldsymbol{\xi} \times \mathbf{e}$, where $\boldsymbol{\xi}$ is a Gaussian white-noise vector, with $\langle\boldsymbol{\xi}\rangle = 0$ and $\langle\boldsymbol{\xi}_i(t)\boldsymbol{\xi}_j(t')\rangle = 2D_r\mathbf{1}\delta_{ij}\delta(t-t')$. The translational and rotational diffusion coefficients, D_t and D_r, are related via $D_t = D_r\sigma^2/3$. The importance of noise is measured by the Péclet number $Pe = V_0/(\sigma D_r)$; we study systems in the range of $9 \leq Pe \leq 272$. Up to $N = 1.5 \times 10^5$ particles are simulated in a cubic box of length L. The density is measured in terms of the global packing fraction $\phi = \pi\sigma^3 N/(6L^3)$. A natural time scale is the rotational relaxation time $\tau_r = 1/(2D_r)$. Despite its simplicity, the model captures the main aspects of various real systems, such as thermo- or diffusiophoretic spherical microswimmers [9,11,18,19] with $Pe \approx 1-80$, persistently swimming spherical colonies of the green algae *Volvox* [20] with $Pe \approx 10^7$ and spherical bacteria *Serratia marcescens* [21] with $Pe \approx 10$.

Phase behaviour. – We first focus on a system with large Péclet number, $Pe = 272$. This system exhibit a remarkable phase behavior as function of the global packing fraction ϕ. Above a critical packing fraction $\phi_c \approx 0.3375$, the system separates into liquid-like and gas-like domains. The morphology of the domains is shown exemplarily in Fig. 1 for different values of ϕ. With increasing volume fraction, the morphology varies from a liquid droplet (Fig. 1(a)) to a bicontinuous structure (Fig. 1(b)) and finally to a gas bubble (Fig. 1(c)).

Figure 2(a) shows the probability distribution $P(\phi_{loc})$ of the local packing fraction ϕ_{loc} as a function of ϕ, where ϕ_{loc} is obtained by Voronoi construction [22]. For $\phi \lesssim \phi_c \approx 0.3375$, the system is essentially homogeneous and $P(\phi_{loc})$ is unimodal. While approaching ϕ_c with increasing ϕ, $P(\phi_{loc})$ broadens (by formation of transient
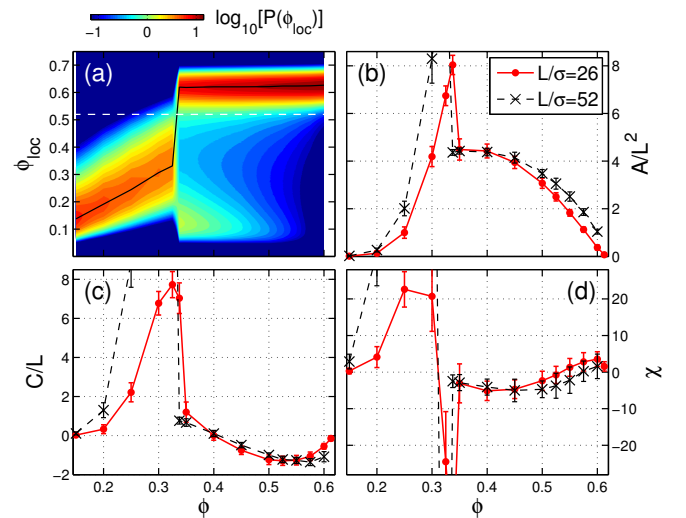

Fig. 2: (color online) (a) Probability distribution $P(\phi_{loc})$ of the local packing fraction ϕ_{loc} as a function of the global packing fraction ϕ for $Pe = 272$ and $L/\sigma = 52$. The most probable ϕ_{loc} is indicated by a solid black line. The density $\phi_{loc} = 0.52$ used as a threshold in Fig. 1 is indicated by a dashed line. (b-d) Morphological analysis of the liquid phase in terms of the Minkowski functionals interface area A (b), integrated mean curvature C (c), and Euler characteristic χ (d).

clusters) and becomes bimodal above ϕ_c. Remarkably, the local packing fraction in the liquid phase $\phi_{liq} \approx 0.62$ is very high, in particular, it is deep within the glassy region ($\phi_G \approx 0.58 \leq \phi_{liq} \leq \phi_{RCP} \approx 0.64$) of passive hard spheres [23,24]. Nevertheless, particles remain mobile and no long-range crystalline order is detected.

The morphological transformations can be characterized by the surface area A, the integrated mean curvature C, and the Euler characteristic χ of the liquid-gas interface. These quantities naturally arise in a geometric characterization, because they are the three (additive) Minkowski functionals in 3D; for details see Ref. [25]. In

the two phase regime, we classify particles as part of the liquid phase if $\phi_{loc} > 0.52$, as indicated by the dashed line in Fig. 2(a). The average values of all functionals, as well as their fluctuations, rise dramatically with increasing $\phi \to \phi_c$ due to enhanced formation of transient spherical ($\chi > 0$) clusters, see Fig. 2(b-d). At ϕ_c, the clusters start to form a percolating network and consequently $\chi < 0$. With increasing $\phi > \phi_c$, the liquid phase forms first a nearly bicontinous structure ($\chi < 0$ and $C < 0$), whose surface is reminiscent of the Schwarz P surface, and finally at high ϕ, gas-phase droplets float in a dense matrix ($\chi > 0$ and $C < 0$). In contrast to an equilibrium system (away from the critical point) the morphology of the gas (or liquid) phase is highly dynamic as is reflected by the large fluctuations of χ, i.e., the structures continuously merge and break as illustrated by the movies `movie1.avi` and `movie2.avi`.

The structure formation of motile hard sphere particles in 3D displays an essential difference compared to 2D: clusters in 2D are crystalline [12] at sufficiently high Pe, while clusters in 3D are fluid. Note that rapidly compressed hard spheres form a glass phase [26], which is absent in 2D for monodisperse discs. This has important consequences for the structure and the dynamics. In both 2D and 3D, particles at the rim of the cluster point inward and hence exert pressure on the interior. However, in the 2D case, the interior cannot easily react to an inhomogeneous pressure distribution because of its finite elastic moduli. This is different for a fluid interior in 3D; a inhomogeneous pressure generates internal currents and a continuous deformation of the structure.

Collective dynamics. – The phase-separated systems reveal an intriguing dynamics within the liquid phase (cf. Fig. 3). Large-scale coherent displacement patterns emerge, with amplitudes and directions strongly varying spatially. In addition, transient swirl-like and jet-like structures appear frequently. Figure 3(a) shows a swirl spanning the whole cluster while Fig. 3(b) displays a large mobile region moving between the gas-phase regions of the system, see supplementary movies `movie3.avi` and `movie4.avi`. This is surprising considering the fact that $\phi_{liq} \approx 0.62 > \phi_G \approx 0.58$.

The particle dynamics displays a strong heterogeneity in space and time. To characterize the correlated dynamics, we adopt the spatio-temporal correlation function [27]

$$C_d(r, \Delta t) = \frac{\left\langle \sum_{i,j\neq i} \mathbf{d}_i \cdot \mathbf{d}_j \, \delta(r - |\mathbf{r}_i - \mathbf{r}_j|) \right\rangle_t}{c_0 \left\langle \sum_{i,j\neq i} \delta(r - |\mathbf{r}_i - \mathbf{r}_j|) \right\rangle_t}, \quad (2)$$

where $\mathbf{d}_i(t, \Delta t) = \mathbf{r}_i(t + \Delta t) - \mathbf{r}_i(t)$ is the displacement of particle i over a lag time Δt and $c_0 = \left\langle \sum_i \mathbf{d}_i^2/N \right\rangle_t$ is a normalization factor. Due to the finite system size we measure $\mathbf{d}$ in the center-of-mass reference frame. In the limit $\Delta t \to 0$, $C_d(r, \Delta t)$ becomes the equal-time spatial velocity correlation function. Moreover, we introduce a
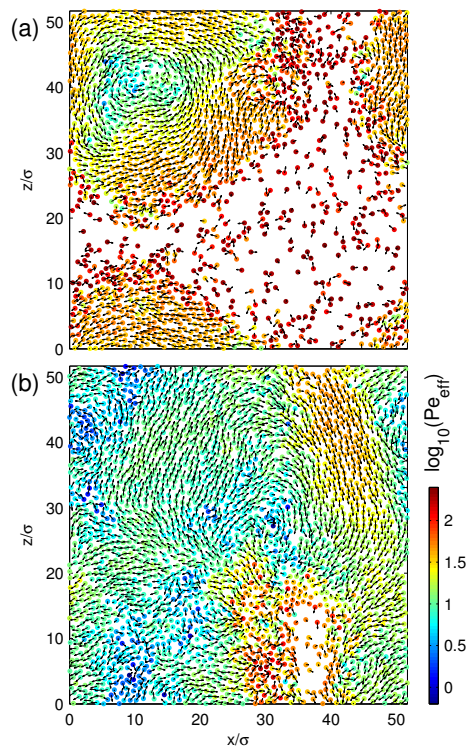

Fig. 3: (color online) Collective motion in the steady state at $Pe = 272$, see supplementary movies `movie3.avi` and `movie4.avi`. Snapshots (slices of thickness σ) of a system (a) just above the clustering transition ($\phi = 0.3375$) and (b) at a high concentration ($\phi = 0.6$). Arrows indicate the direction of the displacements $\mathbf{d}(t, \Delta t) = \mathbf{r}(t + \Delta t) - \mathbf{r}(t)$ over a lag time $\Delta t \approx 0.4\tau_r$. The magnitude $d = |\mathbf{d}|$ is color-coded and is expressed as an effective Péclet number, $Pe_{eff} = d/(\Delta t\sigma D_r)$.

global measure of cooperative motion as

$$\chi_d(\Delta t) = \frac{N}{L^3} \int_{\sigma}^{L/2} 4\pi r^2 C_d(r, \Delta t) \, \mathrm{d}r, \quad (3)$$

which can be interpreted as the average number of coherently moving neighbors. The cooperative motion is not instantaneously present, it rather builds up with time. As shown in Fig. 4(b), $\chi_d(\Delta t)$ first increases, reaches a maximum at $\Delta t = \tau$ (as indicated by symbols), and then decays again. The bell-like shape of $\chi_d(\Delta t)$ is characteristic for the dynamics in dense liquids [27]. The origin of this behavior is that at short times particles move independently in their own cage (low correlation), but gradually they feel the motion of their neighbors and the displacements become correlated over an increasing length scale.

In the following, we focus exemplarily on a system with $\phi = 0.6$, where on average one or two gas-phase droplets float within the dense liquid matix ($\phi_{liq} \approx 0.626$), see Fig. 1(c) and Fig. 3(b); yet our conclusions are valid for most $\phi > \phi_c$. Figure 4(a) shows C_d for various system sizes L at the time τ of maximal cooperativity. The correlations exhibit an initial power-law decay, followed by an exponential decay, and become finally negative. The an-
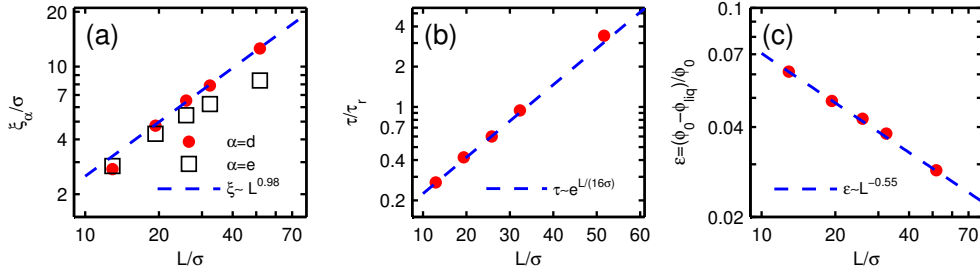
Fig. 5: (color online) (a) Correlation lengths of the displacements $\xi_d(\tau)$ and the orientations ξ_e as a function of system size L. (b) Exponential grow of the build-up time τ with L. (c) Local density of the liquid phase ϕ_{liq} increases with L. The same parameter as in Fig. 4, $\phi = 0.6$ and $Pe = 272$.
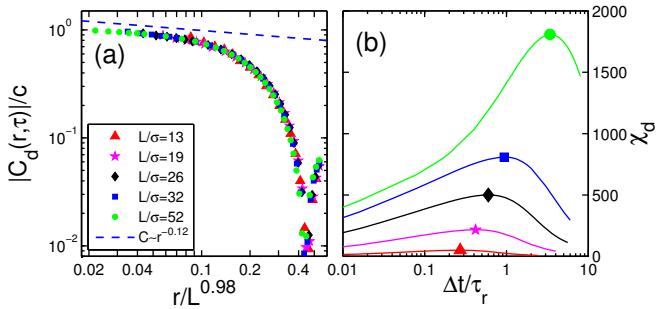

Fig. 4: (color online) (a) Modulus of the spatial displacement correlation function $C_d(r, \Delta t = \tau)$ as a function of $r/L^{0.98}$ for $\phi = 0.6$ and $Pe = 272$. We show C_d at the time τ of maximal cooperativity. C_d is scaled by $c = 0.46, 0.56, 0.57, 0.52, 0.33$ for $L/\sigma = 13, 19, 26, 32, 52$, respectively. (b) Cooperativities $\chi_d(\Delta t)$ of the various system sizes L. The symbols indicate τ.

ticorrelation corresponds to a backflow of particles, which can be attributed to the incompressibility of the liquid phase.

Fitting a stretched exponential function (along with a power law),

$$C(r) \sim r^{-\alpha} \exp\left[-(r/\xi)^{\beta}\right], \qquad (4)$$

to the data yields the exponents $\alpha = 0.12$ and $\beta = 1.3$, and a (nearly) linear increase of the correlation length $\xi_d(\tau)$ with L (cf. Fig. 5(a)). The good data collapse in Fig. 4(a) with scaled distance $r/L^{0.98}$ indicates the existence of an universal finite-size scaling function, at least over the considered range of system sizes. Furthermore, for large L, the system is expected to become scale invariant, with a power-law decay of $C_d(r)$. A similar behavior has been discussed in other active systems [28, 29], however, with a notable polar alignment mechanisms, such as starling flocks [28] and motile bacteria colonies [29].

Active fluids with repulsive interactions between particles resemble in some aspects passive fluids in equilibrium with attractive interactions, e.g., both display a phase separation [14–16, 30, 31]. However, in many other aspects, active fluids behave very differently. First, we find an increase of the local density of the liquid phase ϕ_{liq} with

system size L at fixed ϕ as $(\phi_0 - \phi_{liq})/\phi_0 \sim L^{-1/\delta}$ with $\delta \approx 1.8$ and $\phi_0 \approx 0.645$ (note that the actual ϕ is somewhat larger due to the Yukawa part of the potential), see Fig. 5(c). Such a *self-compaction* is a clear non-equilibrium feature of active fluids. Second, we observe a strong increase of the build-up time τ with increasing L, namely, $\tau \sim \exp\left(L/\xi_0\right)$ with $\xi_0 = 16\sigma$, see Fig. 5(b). Hence, long-living, coherently moving domains are expected for large systems. In fact, these two observations can be related to each other by the physics of dense passive fluids near the glass transition. It is generally accepted that the relaxation time (proportional the build-up time) near the glass transition obeys the generalized Vogel-Fulcher-Tammann law, $\tau \sim \exp\left[A(\phi_0/(\phi_0 - \phi_{liq}))^{\delta}\right]$ with $\delta = 1 - 2$ and $\phi_0 = 0.614 - 0.637$ [23]. However, particle activity fluidizes the glass phase and shifts the glass transition to $\phi_0 = 0.6573$ with $\delta = 1$ in the limit $Pe \to \infty$ [32]. Thus, the large correlation times τ for large systems can be understood as a consequence of (active) self-compaction.

Intuitively, a strong correlation between the particle orientation $\mathbf{e}$ and its direction of motion $\mathbf{d}/|\mathbf{d}|$ can be expected. However, we find only a weak relation between the cooperative motion and orientation correlations. The latter can be characterized by the (equal-time) correlation function $C_e(r)$, where the displacement vector $\mathbf{d}$ is replaced by the orientation vector $\mathbf{e}$ in Eq. (2). In addition, a global measure χ_e of orientation correlations can be defined in analogy to χ_d in Eq. (3). Although, C_e signals long-range correlations, however, weaker than C_d, with $\xi_e < \xi_d$ (see Fig. 5(a)), the orientation correlations, which originate from small regions of polar order at the gas-liquid interface, are very weak and χ_e is an order of magnitude smaller than $\chi_d(\tau)$.

Motivated by snapshots (Fig. 3) and movies (`movie3.avi` and `movie4.avi`), we propose the following mechanism behind the observed collective dynamics. Consider first a smooth (flat) interface between the gas and liquid phase: fast moving gas-phase particles bump into the interface and remain there until rotational diffusion leads to an approximately parallel orientation of $\mathbf{e}$ to the interface [33]. In concave regions of a curved interface, however, the reorientation of $\mathbf{e}$ requires more
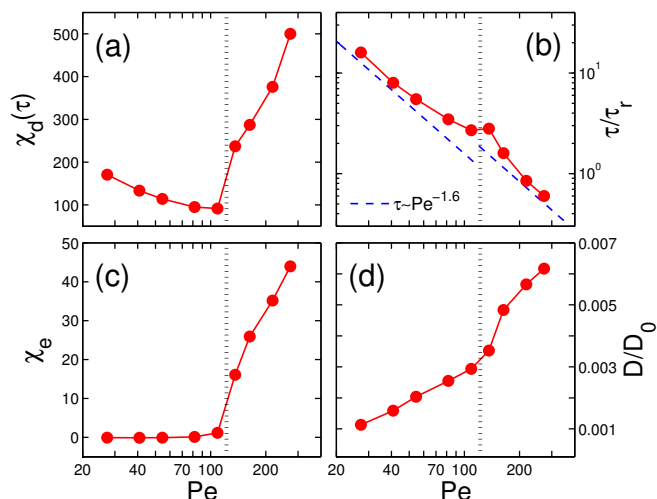
Fig. 6: (color online) (a) Cooperativity $\chi_d(\tau)$, (b) build-up time τ, (c) global polar correlation χ_e and (d) long-time diffusion constant D (normalized by $D_0 = D_t + V_0^2/(6D_r)$) as a function of Pe for the packing fraction $\phi = 0.6$ and the system size $L/\sigma = 26$. The dashed line indicates $Pe_{c,1} \approx 120$.

Fig. 7: (color online) Phase diagram of the active suspension spanned by Pe and ϕ. Symbols denote the homogenous liquid phase ($\circ$), the gas-liquid coexistence ($\square$) and the crystal-gas coexistence ($\triangleright$). The equilibrium transition points of hard-sphere freezing ($\phi_F = 0.494$), melting ($\phi_M = 0.545$), glass-transition point ($\phi_G \approx 0.58$), and random close packing ($\phi_{RCP} \approx 0.64$), are marked by F, M, G, RCP, respectively. The most probable ϕ_{loc} is color-coded, i.e., in the two-phase region one can read off the density of the dense liquid phase ϕ_{liq}. The horizontal and the vertical short dashed lines correspond to results presented in Fig. 2 and Fig. 6, respectively. The solid line marks $Pe_c(\phi)$ which is proportional to Eq. (5).

time until escape is possible, i.e., particles are effectively trapped. By contrast, particles in convex regions (protrusions) slide easily into a neighboring concave regions. This self-amplifying process accumulates particles with distinct polar order in concave regions and thereby triggers streams of orientationally disordered particles deep inside the liquid phase, which explains the much weaker correlations in particle orientations than in displacements. Due to mass conservation, the particles stream into a neighboring gas droplet or toward the droplet which itself activated the flow. As a result, further deformations of droplets are produced and hence new instabilities are induced.

So far we have focussed on the large Péclet number $Pe = 272$. However, variation of the activity substantially affects the structure and dynamics of the suspension. We illustrate this behavior for $\phi = 0.6$ (see vertical dashed line in Fig. 7). By decreasing Pe we pass three regions, a liquid-gas phase at high Pe, a homogeneous liquid phase below $Pe_{c,1} \approx 120$, and finally a crystal-gas phase below $Pe_{c,2} \approx 20$. In the homogeneous phase $Pe_{c,2} < Pe < Pe_{c,1}$, there is no polar order and $\chi_e \approx 0$, see Fig. 6(c). The dynamical behavior of the systems change drastically while crossing $Pe_{c,1}$. As displayed in Fig. 6(a), the maximal cooperativity $\chi_d(\tau)$ is nearly constant below $Pe_{c,1}$ and increases strongly with Pe above $Pe_{c,1}$. In addition, activity substantially speeds up the build-up time τ, namely, $\tau \sim Pe^{-1.6}$ as shown in Fig. 6(b). As a result, collective motion below $Pe_{c,1}$ appears on time scales $\tau \gg \tau_r$ and becomes increasingly reminiscent of an passive supercooled fluid [27]; note that $\tau = \infty$ for $Pe = 0$ since $\phi > \phi_G$ [23]. Finally, the particle dynamics is drastically slowed down for $Pe < Pe_{c,2}$, where
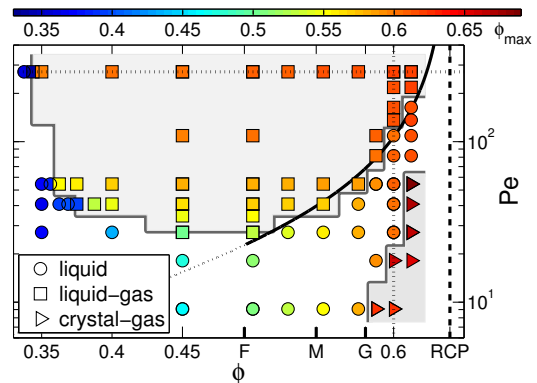
the system starts to freeze, as indicated in the phase diagram in Fig. 7. In Fig. 6(d), we show the diffusivity D normalized by the corresponding value of a free active particle, $D_0 = D_t + V_0^2/(6D_r)$. Although the system is above ϕ_G, D is finite and is an increasing function of Pe. The latter suggests a shift of the glass transition to larger ϕ with increasing activity [32, 34–36].

We collect all our results in a phase diagram spanned by Pe and ϕ, see Fig. 7. For high Pe, the homogenous phase is unstable over a broad range of packing fractions ϕ, as explained above. The unstable range decreases with decreasing Pe (the lower bound is predicted to obey $\phi_c \sim \phi_1 + \phi_2/Pe$ [12,37] with constants $\phi_{1,2}$). Below $Pe_{min} \approx 30$ phase separation disappears for all ϕ. Except for large ϕ and low Pe, where crystalline domains are formed, the dynamics is fluid-like. The surprising feature of the phase diagram at high ϕ, the presence of a homogeneous fluid phase in the gap between the liquid-gas and the crystal-gas coexistence, was very recently also observed in an active soft-disk system in 2D [37]. Finally, we expect jamming to occur for $\phi \to \phi_{RCP}$ in the limit of $Pe \to \infty$.

The phase separation as a function of ϕ and Pe can be understood as follows. The pressure of a hard sphere fluid increases with ϕ and diverges at RCP for the metastable branch as

$$p_{HS} = -\frac{6k_B T}{\pi \sigma^3} \phi^2 \frac{\mathrm{d}}{\mathrm{d}\phi} \ln \left\{ \left[(\phi_{RCP}/\phi)^{1/3} - 1 \right]^3 \right\}, \quad (5)$$

according to the free volume theory [24]. Self-propelled particles at low ϕ easily overcome this pressure, coagulate due to their slow-down during collisions (overdamped

dynamics) and hence form clusters. The density within the cluster, ϕ_{liq}, adjusts such that $p_{HS}(\phi_{liq})$ balances the active pressure p_a. An initially homogenous system can only phase separate if the active pressure $p_a \sim \gamma_t V_0/\sigma^2$ exceeds $p_{HS}(\phi)$, this explains the existence of a boundary, $Pe_c(\phi)$, between the liquid-gas coexistence and the homogenous liquid phase at high ϕ, see solid line in Fig. 7; a similar argument was used in Ref. [37] in the context of soft disks.

Summary and Conclusions. – Suspension of active particles without an alignment rule exhibit on broad range of fascinating structural and collective dynamical effects. In particular, we find a phase separation in a gas phase and a liquid phase with a highly dynamic domain structure. The interior dynamics of the liquid domains displays a strong heterogeneity in space and time. Surprisingly, the dynamical behavior is highly collective, despite the absence of an alignment mechanism. This collective dynamics can only arise from a spatial sorting of particles with similar orientation. The reorientation of particles at an interface provides such a sorting mechanism.

Several interesting questions arise from our results. In particular, the crossover from the equilibrium phase behavior to the regime at low Pe deserves further attention. The mechanism of self-compaction, which does not seem to be explainable easily from neither an effective active particle attraction nor from the compressive interface layer, has to be elucidated. Studies of active fluids at low Pe may also shed light on the dynamics in glassy systems in a complementary way to external fields like shear.

$* * *$

REFERENCES

[1] Vicsek T. and Zafeiris A., *Phys. Rep.*, **517** (2012) 71.
[2] Angelini T. E., Hannezo E., Trepat X., Marquez M., Fredberg J. J. and Weitz D. A., *Proc. Natl. Acad. Sci. USA*, **108** (2011) 4714.
[3] Kearns D., *Nat. Rev. Microbiol.*, **8** (2010) 634.
[4] Wensink H. H., Dunkel J., Heidenreich S., Drescher K., Goldstein R. E., Löwen H. and Yeomans J. M., *Proc. Natl. Acad. Sci. USA*, **109** (2012) 14308.
[5] Peruani F., Deutsch A. and Bär M., *Phys. Rev. E*, **74** (2006) 030904.
[6] Yang Y., Marceau V. and Gompper G., *Phys. Rev. E*, **82** (2010) 031904.
[7] Lauga E. and Powers T. R., *Rep. Prog. Phys.*, **72** (2009) 096601.
[8] Fily Y. and Marchetti M. C., *Phys. Rev. Lett.*, **108** (2012) 235702.
[9] Theurkauff I., Cottin-Bizonne C., Palacci J., Ybert C. and Bocquet L., *Phys. Rev. Lett.*, **108** (2012) 268303.
[10] Palacci J., Sacanna S., Steinberg A. P., Pine D. J. and Chaikin P. M., *Science*, **339** (2013) 936.
[11] Buttinoni I., Bialké J., Kümmel F., Löwen H., Bechinger C. and Speck T., *Phys. Rev. Lett.*, **110** (2013) 238301.
[12] Redner G. S., Hagan M. F. and Baskaran A., *Phys. Rev. Lett.*, **110** (2013) 055701.
[13] Bialké J., Löwen H. and Speck T., *EPL*, **103** (2013) 30008.
[14] Speck T., Bialké J., Menzel A. M. and Löwen H., *arXiv preprint arXiv:1312.7242*, (2013) .
[15] Stenhammar J., Marenduzzo D., Allen R. J. and Cates M. E., *Soft Matter*, (2014) in press.
[16] Cates M. E. and Tailleur J., *EPL*, **101** (2013) 20010.
[17] Bialké J., Speck T. and Löwen H., *Phys. Rev. Lett.*, **108** (2012) 168301.
[18] Howse J. R., Jones R. A. L., Ryan A. J., Gough T., Vafabakhsh R. and Golestanian R., *Phys. Rev. Lett.*, **99** (2007) 048102.
[19] Jiang H.-R., Yoshinaga N. and Sano M., *Phys. Rev. Lett.*, **105** (2010) 268302.
[20] Drescher K., Leptos K. C., Tuval I., Ishikawa T., Pedley T. J. and Goldstein R. E., *Phys. Rev. Lett.*, **102** (2009) 168101.
[21] Rabani A., Ariel G. and Be'er A., *PLoS ONE*, **8** (2013) e83760.
[22] Rycroft C. H., *Chaos*, **19** (2009) 041111.
[23] Brambilla G., El Masri D., Pierno M., Berthier L., Cipelletti L., Petekidis G. and Schofield A. B., *Phys. Rev. Lett.*, **102** (2009) 085703.
[24] Kamien R. D. and Liu A. J., *Phys. Rev. Lett.*, **99** (2007) 155501.
[25] Michielsen K. and Raedt H. D., *Phys. Rep.*, **347** (2001) 461 .
[26] Davis K. E., Russel W. B. and Glantschnig W. J., *Science*, **245** (1989) 507.
[27] Doliwa B. and Heuer A., *Phys. Rev. E*, **61** (2000) 6898.
[28] Cavagna A., Cimarelli A., Giardina I., Parisi G., Santagati R., Stefanini F. and Viale M., *Proc. Natl. Acad. Sci. USA*, **107** (2010) 11865.
[29] Chen X., Dong X., Be'er A., Swinney H. L. and Zhang H. P., *Phys. Rev. Lett.*, **108** (2012) 148101.
[30] Tailleur J. and Cates M. E., *Phys. Rev. Lett.*, **100** (2008) 218103.
[31] Stenhammar J., Tiribocchi A., Allen R. J., Marenduzzo D. and Cates M. E., *Phys. Rev. Lett.*, **111** (2013) 145702.
[32] Ni R., Cohen Stuart M. A. and Dijkstra M., *Nat. Commun.*, **4** (2013) 2704.
[33] Elgeti J. and Gompper G., *EPL*, **101** (2013) 48003.
[34] Kranz W. T., Sperl M. and Zippelius A., *Phys. Rev. Lett.*, **104** (2010) 225701.
[35] Berthier L. and Kurchan J., *Nat. Phys.*, **9** (2013) 310.
[36] Berthier L., *arXiv preprint arXiv:1307.0704*, (2013) .
[37] Fily Y., Henkes S. and Marchetti M. C., *Soft Matter*, (2013) in press.